Journal of Manufacturing Processes 107 (2023) 515–528

Contents lists available at ScienceDirect

Journal of Manufacturing Processes

journal homepage: www.elsevier.com/locate/manpro

MD simulation of chemically enhanced polishing of 6H-SiC in aqueous H_2O_2

Shengyao Yang [a], Xuliang Li [a], Yitian Zhao [a], Md Al-amin [a], Lisbeth Grøndahl [b,*], Mingyuan Lu [a,*], Chi Fai Cheung [c], Han Huang [a,*]

[a] School of Mechanical & Mining Engineering, The University of Queensland, Brisbane, QLD 4072, Australia
[b] School of Chemistry and Molecular Biosciences, The University of Queensland, Brisbane, QLD 4072, Australia
[c] Department of Industrial and Systems Engineering, State Key Laboratory of Ultra-precision Machining Technology, The Hong Kong Polytechnic University, Kowloon, Hong Kong

ARTICLE INFO

Keywords:
Polishing
Silicon carbide
ReaxFF MD
Chemical effect
Material removal

ABSTRACT

Chemical enhanced polishing (CEP) is a widely employed final process for achieving precise surface shaping and planarization of semiconductor wafers. However, determining the chemical effect involved in material removal through experimental means is extremely challenging. In this study, we conducted reactive force field (ReaxFF) molecular dynamics (MD) simulations to gain insight into the chemical effects of CEP using an aqueous hydrogen peroxide (H_2O_2) diamond suspension as a polishing medium for 6H-SiC single crystals. The inclusion of aqueous H_2O_2 resulted in the formation of Si—O—H and C—O—H species, which are comparatively easier to remove through mechanical abrasion. Furthermore, an increase in H_2O_2 concentration was found to enhance the material removal. The MD simulations also revealed that the chemical effects on the Si-face of 6H-SiC were more pronounced than those on the C-face due to the generation of a greater number of Si—O species and the favourable atomic structure of the Si-face for chemical removal. The results showed that the material remove rate on the Si-face is greater than that on the C-face during polishing, aligning with the findings from MD simulation. Furthermore, a systematic experimental study was carried out to examine the influence of various conditions on material removal rate and surface quality in both polishing and lapping processes.

1. Introduction

Single crystal silicon carbide (SiC) is a highly promising third-generation semiconductor material [1,2]. With its wide energy band gap, excellent chemical inertness, high breakdown electric field, and superior thermal conductivity [3–7], SiC finds extensive applications in power electronics devices like diodes and field effect transistors [8], hybrid electric vehicles [9], solar photovoltaics [10], railcar tractions [11], power transportation [12], and biosensors [13]. To achieve high-quality SiC components for electronic and optoelectronic applications, the shaping of bulk SiC necessitates a series of abrasive machining processes [14,15] However, the machining of SiC poses significant challenges due to its extreme hardness and brittleness [16]. Chemically enhanced machining techniques such as chemically enhanced lapping (CEL) [17] and chemical mechanical polishing (CMP) [18,19] are commonly employed as the final steps for surface finishing.

Previous research has predominantly focused on experimental investigations concerning material removal in the chemical mechanical polishing (CMP) of SiC. For instance, a study conducted in 1997 highlighted the role of increased OH group concentration in the polishing media, facilitating Si—C oxidation during the CMP of SiC single crystals [19]. The presence of silicon oxycarbide species on the polished SiC surfaces further indicates oxidation during the polishing process [20]. Similar oxidation phenomena have been observed in UV-light assisted CMP [21]. These studies aimed at optimizing the process through abrasive and slurry selection, as well as technical approaches to enhance chemical effects in polishing [22–28]. However, limited attention has been given to comprehending the underlying mechanism of the chemical effect, primarily due to the constraints of experimental characterization techniques in monitoring changes during the lapping process. Previous investigations have yielded contradictory observations regarding SiC crystal polishing. Some studies reported higher chemical activity on the Si-face, resulting in a greater removal rate [29–31], while others demonstrated higher material removal efficiency on the C-face

* Corresponding authors.
E-mail addresses: l.grondahl@uq.edu.au (L. Grøndahl), m.lu1@uq.edu.au (M. Lu), han.huang@uq.edu.au (H. Huang).

https://doi.org/10.1016/j.jmapro.2023.10.056
Received 19 June 2023; Received in revised form 18 August 2023; Accepted 21 October 2023
Available online 1 November 2023
1526-6125/© 2023 The Authors. Published by Elsevier Ltd on behalf of The Society of Manufacturing Engineers. This is an open access article under the CC BY license (http://creativecommons.org/licenses/by/4.0/).

[32–36]. Consequently, there is a clear need for a deeper understanding of the material removal mechanism in the CMP of SiC.

MD simulation has emerged as a valuable tool for understanding material deformation and removal at the nanoscale [37–44]. However, traditional MD simulations do not account for chemical effects in mechanical removal since they assume fixed connectivity and employ harmonic potential terms that are inadequate for simulating chemical reactions. In contrast, the ReaxFF interatomic potential, developed based on quantum chemistry principles (QC), enables the simulation of bond breakage and formation, making it a powerful tool for studying chemical effects [45–47]. The ReaxFF force field has been extensively used to investigate tribochemical reactions and atomic removal mechanisms in CMP [48–59].

For instance, Wen et al. [48,49] explored the tribochemical wear mechanism of silicon in humid air and observed the formation of Si—O—Si bonds through reactions between Si—O—H from abrasives and Si—O—H from water with surface Si atoms, facilitating the breaking of Si—Si bonds in the silicon substrate. Chen et al. [50] investigated the removal mechanism of (100) silicon during CMP and demonstrated the feasibility of removing a single atomic layer. Wang et al. [51] systematically studied the material removal mechanisms of Si (110) surface during CMP. Guo and Yuan et al. [52–54] conducted extensive research on the chemical mechanical removal mechanisms of diamond and quartz glass in CMP. He et al. [55] examined the chemical mechanical interaction in CMP using a silica abrasive particle. Wang et al. [60] studied the wear of a water-lubricating SiC surface, revealing the mechanical role of water in reducing adhesive wear and its chemical role in reacting with SiC, resulting in the triboemission of surface SixHyOz groups. Previous studies have also explored the polishing of materials like copper [56,57], silica [58], and diamond-like carbon (DLC) [59]. These investigations demonstrate the efficacy of ReaxFF MD in simulating the combined effects of chemical reactions and mechanical abrasion involved in polishing.

This study utilizes ReaxFF MD simulation to investigate the impact of the chemical effect on material removal during a chemically enhanced polishing (CEP) process of 6H-SiC. The CEP process employs an aqueous H_2O_2 suspension with diamond abrasives as additives. It is worth noting that CEP is distinct from conventional CMP, as CEP aims to improve removal efficiency rather than surface integrity. This study provides unique insights by focusing on the specific role of H_2O_2 and its concentration in the removal performance of CEP. The investigation offers valuable understanding of the material removal mechanism on the (0001) and $(000\bar{1})$ faces of the 6H-SiC crystal.

2. Simulation method

The MD simulation was conducted in the large-scale atomic/molecular massively parallel simulator (LAMMPS) [61]. OVITO software was used for post-processing and visualisation [62]. Two types of MD models were constructed: one was to understand the chemical effect only, described in detail later in Section 2.2, while the other was used to simulate both chemical and mechanical effects, which is depicted in Section 2.3. All the processes were simulated at room temperature (300 K) condition controlled by the Nosé-Hoover thermostat [63]. Periodic boundary conditions were applied in both length (x-) and width (y-) directions, and a free boundary condition was applied in the thickness (z-) direction. To prevent atoms from escaping in the z-direction, a reflective wall was established at the boundary. A timestep of 0.25 femtoseconds (fs) was applied for all the simulations.

2.1. ReaxFF reactive force field

The ReaxFF reactive force field is a bond-order-dependent potential. The connectivity between atoms is updated and modified at every time step. ReaxFF can describe the bond generation and breakage involved in material removal, and thus the dynamics of a chemical reaction at atomical scale [47]. The general description of the ReaxFF potential is given by:

$$E_{sys} = E_{bond} + E_{val} + E_{tor} + E_{over} + E_{under} + E_{lp} + E_{vdWaals} + E_{coulomb} \quad (1)$$

where E_{sys}, E_{bond}, E_{val}, E_{tor}, E_{over}, E_{under}, E_{lp}, $E_{vdWaals}$ and $E_{coulomb}$ are the energies of the entire system, bond, valence angle, torsion angle, over-coordination penalty, under-coordination penalty, lone-pair, van der Waals and Coulomb bonds, respectively. The electron equilibration method (EEM) [64] is employed to calculate the atomic charges in the ReaxFF.

The force field used in this study is the ReaxFF potential reported previously [48]. The details of the potential function can be found in the supplementary documents. This potential function was adapted for studying the tribochemical wear in a CEP process for 6H-SiC. The stability of expressed 6H-SiC by this ReaxFF potential function is discussed in this work. Table 1 provides a comparison of the lattice parameters and cohesive energy for 6H-SiC, which includes results obtained using the ReaxFF potential and contrasts them with values derived from the classical Tersoff [65] and Vashishta [66] potential energy functions on the same model, as well as data from the density functional theory (DFT) modeling and previous experimental studies [67,68]. The ReaxFF potential function is considered applicable since, following its application, the structure remained stable, and the differences in lattice parameters compared to those obtained using other potential functions or experimental reference values fall within the tolerance.

2.2. The chemical model

The MD model for simulating the chemical effect only comprises a 6H-SiC substrate that consists of C and Si atoms, and an aqueous suspension of different H_2O and H_2O_2 contents, as shown in Fig. 1. Note that diamond abrasives are not included in the chemical model, and the H_2O_2 concentration is altered by varying the H_2O_2/H_2O ratio from 11 wt % to 21 wt%, to examine its chemical effect, as shown in Table 2. All the molecules in the aqueous layer are allowed to participate in a chemical reaction. The substrate contains 1458C atoms and 1458 Si atoms. The atoms in the bottom two layers are fixed and the atoms above the fixed layers are free to move when they are involved in a chemical reaction. The system was equilibrated using the NVT ensemble [69] at a timestep of 0.25 femtoseconds over a period of 100 picoseconds (ps) to ensure the completion of the chemical reactions, or until there was no further change in the number of species.

2.3. The CEP model

The CEP model consists of three parts: diamond abrasive, aqueous H_2O_2 polishing media and SiC substrate, as shown in Fig. 2. The model has a size of $29.1 \times 50.4 \times 37$ Å^3. The diamond abrasive is composed of 10 atomic layers of 2240C atoms, which are allowed to move as a whole horizontally and vertically to simulate the motion of an individual abrasive during polishing. The top two layers of the abrasive atoms are fixed, acting as a rigid body, while the remaining C atoms are free to move under mechanical loading following the Newton's Second Law of Motion or the driving force generated by chemical reactions. The setup of aqueous H_2O_2 solution and SiC substrate is the same as that in the

Table 1
Comparison of the results for SiC obtained using ReaxFF potential with those obtained from other methods, including Tersoff, Vashishta potential, DFT and experiments.

Parameters	ReaxFF	Tersoff [65]	Vashishta [66]	DFT & Exp.
Lattice constant a (Å)	3.237	3.079	3.08	3.077 [67]
Lattice constant c (Å)	15.891	15.117	15.121	15.108 [67]
Cohesive energy (eV)	6.283	6.164	6.331	6.66 [68]

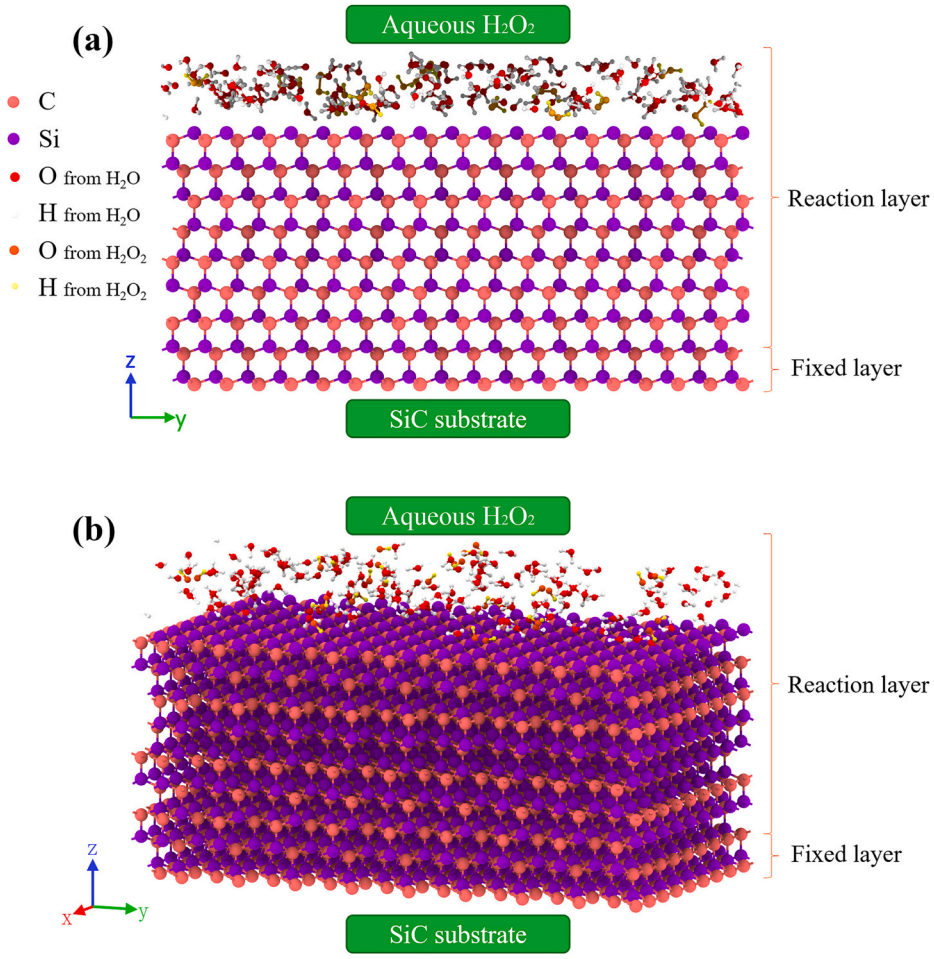

Fig. 1. The (a) 2D and (b) 3D chemical model of 6H-SiC and aqueous H_2O_2. The bottom two layers of SiC are fixed, but those above the fixed layer are free to move if they participate in the chemical reactions.

Table 2
H_2O_2 concentrations and the corresponding numbers of H_2O and H_2O_2 molecules in the chemical model.

H_2O_2 concentration (wt%)	Number of H_2O	Number of H_2O_2
21	140	20
16	150	15
11	160	10

chemical model shown in Fig. 1. The simulation parameters as well as the set-up parameters are summarized in Table 3. The system was equilibrated using the NVT ensemble [69] at a timestep of 0.25 fs for 100 ps. Upon equilibrium, the model starts to simulate a CEP process based on the following procedures: (i) the diamond abrasive approaches the substrate vertically (along *z*-direction); with a gradual increase in pressure, the aqueous layer was compressed until the normal pressure reached 40 GPa, which was selected as the criterion for effective SiC removal during the simulation; (ii) the system is equilibrated for another 10 ps, so that the system reaches a new stable state; (iii) the diamond abrasive then translates along y-direction at a speed of 50 m/s for 200 ps under the NVT ensemble to simulate the polishing action; (iv) finally, the diamond abrasive withdraws from the substrate surface.

2.4. Postmortem analysis of MD simulation

To quantitatively characterize the atomic disorder caused by the chemical effect, displacement of atoms in the MD models can be calculated using [49]:

$$d = \sqrt{(x - x_0)^2 + (y - y_0)^2 + (z - z_0)^2} \tag{2}$$

where d is the displacement of each individual atom, (x_0, y_0, z_0) is the initial coordinate of the atom, (x, y, z) is the real time position during CEP. For a 6H-SiC single crystal with a diamond structure, Si—C bond length is 1.98 Å, and the atomic distance of Si—Si and C—C are both 3.24 Å [70]. An atom being removed from the 6H-SiC substrate was assumed to meet the criterion of $d > 4.5$ Å, which is approximately 1.5 times the maximum atomic distance. It should be noted that the disorder caused by abrasive sliding may add complexity and inaccuracy to the calculation, which means that not all atoms with $d > 4.5$ Å are truly removed [55]. Nevertheless, the quantitative measurement can assess the level of disorder reasonably.

Identify Diamond Structure [71], an analysis modifier that is integrated in the OVITO software, was used to characterize the structural changes of 6H-SiC that has a pristine diamond structure. This analysis modifier can find atoms that are arranged in a cubic or hexagonal diamond lattice by analysing the local environment of each atom up to the second neighbor shell. In OVITO, atoms are displayed using the calculated positions against time. This enables us to visualize relevant atom movements at any time. To illustrate the removal of Si and C atoms in the model, the distance between the abrasive and the substrate is exaggerated in the figure, but the atomic distance within the abrasive and substrate remained constant. Snapshot views were taken from the vertical direction of sliding on the substrate.

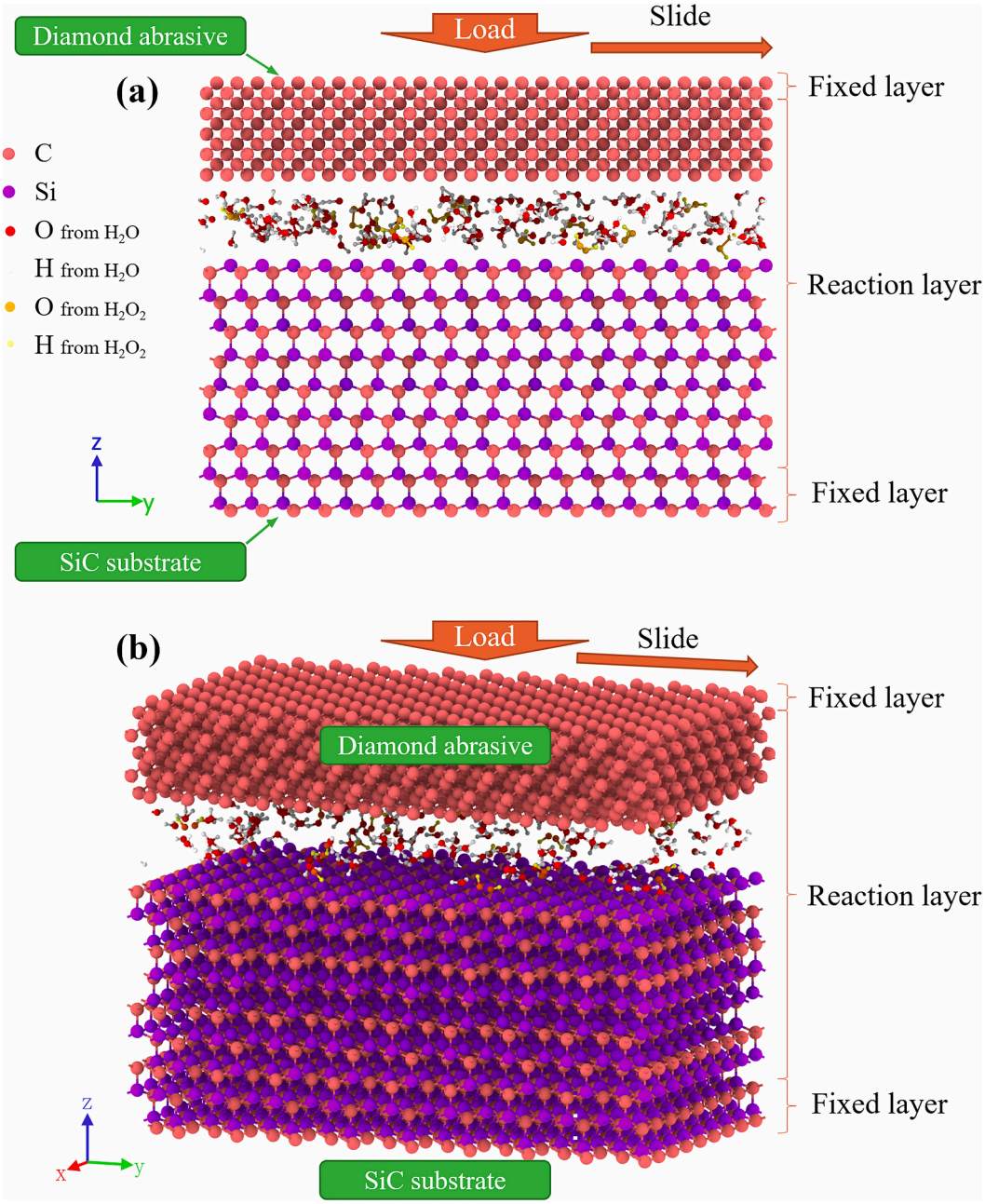

Fig. 2. The (a) 2D and (b) 3D CMP model of 6H-SiC, aqueous H_2O_2 and a diamond abrasive.

Table 3
MD parameters used in the CEP model.

Parameters	Values
Directions ($x \times y \times z$)	$\langle 11{-}20\rangle \times \langle 1{-}100\rangle \times \langle 0001/000\text{-}1\rangle$
Dimensions (Å^3)	29.1 × 50.5 × 37
Number of Atoms	5656–5676
Sliding time (ps)	200
Sliding speed (m/s)	50
Sliding pressure (GPa)	40
Boundary condition	p p f
Sliding distance (nm)	10
Equilibration temperature (K)	300
Time step (fs)	0.25

2.5. Experimental setup

Lapping and polishing tests were carried out on a precision automated polisher (TegraPol-31, Struers, Denmark), as illustrated in Fig. 3. The 6H-SiC wafers (supplied by MTI Corporation, USA) have dimensions of 5 × 5 × 0.33 mm^3. Suspensions of diamond and graphene oxide (GO) nanosheets were prepared following a protocol developed in our lab [20]. The diamond abrasives have an average particle size from 250 nm to 3000 nm and were used at a concentration of 1.00 wt%. Additionally, the concentration of GO was 0.25 wt%. It should be noted that GO was used as the oxidant in the experiment, while H_2O_2 was used in the MD simulation. This is because: (1) using GO to supply OH radicals is much more environmentally friendly than using H_2O_2, (2) the oxidation mechanisms of GO water suspension and H_2O_2 are very similar, as both involve the generation of OH radicals to induce oxidation on SiC [17,20], and (3) the currently available resource for computation cannot

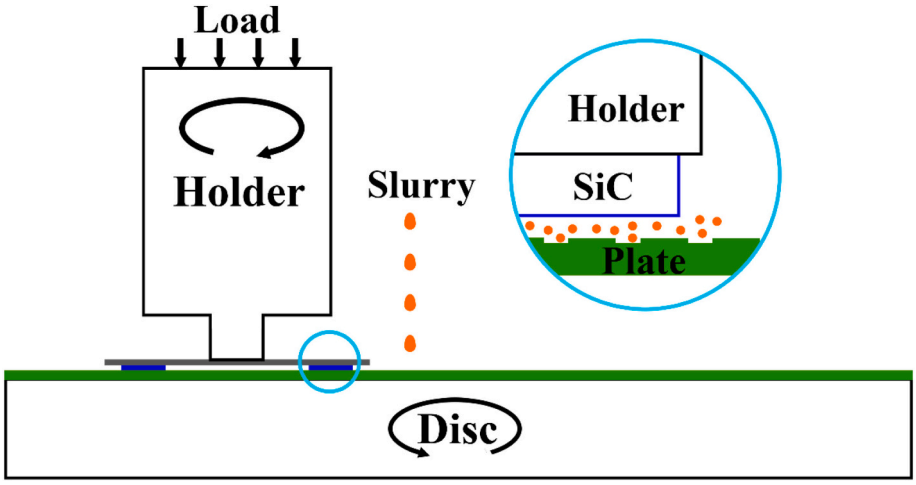

Fig. 3. Schematic illustration of the lapping/polishing system.

support the MD simulation of GO. The MD-Largo metal-resin composite plate (Struers, Denmark) was used as the lapping disc, and the MD-Nap fabrics plate (Struers, Denmark) was used as the polishing disc. During lapping and polishing, the disc and the holder rotated in the opposite directions and detailed operation parameters are shown in Table 4. Surfaces of the polished samples were examined using a confocal microscope (LEXT OLS4100, Olympus, Japan) and an atomic force microscope (AFM, Dimension XR, Bruker, USA) and the surface roughness in terms of arithmetic mean height (*Sa*) was measured. The thickness of the samples was measured using a Spiral Micrometer (MDC-1″ PXT, Mitutoyo, Japan) prior to and after lapping or polishing, which was used to calculate the *MRR*. Each test was repeated thrice, and averaged values and standard deviations were determined based on the test results. Nanoindentation and nanoscratching tests were performed on an in-situ indenter (ASA-ECO, Alemnis AG, Switzerland) and a Triboindenter (TI900, Hysitron Inc., US), respectively, for characterizing the mechanical properties of 6H-SiC.

3. Simulation results

3.1. Chemical effect of aqueous H_2O_2

Fig. 4 shows the cross-sectional views of the (0001) Si-face of 6H-SiC after being exposed to H_2O_2 solution (16 wt%) for a period of 40 and 100 ps. In both cases, Si—O—H and Si—H species can be observed on the SiC surface. However, no C—H or C—O—H species are found as the water and H_2O_2 does not 'intrude' the SiC where C atoms are not exposed on the (0001) Si-face. It should be noted in Fig. 4(a) that H_2O_2 molecules are still visible at 40 ps, but they are no longer observed after 100 ps, as shown in Fig. 4(b), indicating the completion of the chemical reaction involving H_2O_2. This is in consistent with previous numerical and experimental studies where it was found that Si atoms on the SiC surface could be terminated by forming Si—H and Si—O—H end groups after chemical reaction [31,72–76].

The remaining H_2O and H_2O_2, as well as the Si—O—H and Si—H species formed during the chemical reaction, were plotted against reaction time in Fig. 5 for various H_2O_2 concentrations, as well as pure water. These graphs were obtained by counting the number of each species in real time at each timestep via programming methods. The number of water (5a) and H_2O_2 (5b) molecules decreased in the initial stage of the reaction, Si—O—H and Si—H species increased correspondingly with the progress of the reaction, all reaching the respective saturated values after approximately 40 ps. Increasing the H_2O_2 concentration resulted in the formation of more Si—O—H, but less Si—H species.

Water generates an equal amount of Si—O—H and Si—H species, which is consistent with a previous Ab Initio MD study that showed a 'cooperative hydrogen transfer' mechanism accounting for this observation [75]. The presence of H_2O_2 enhanced the generation of Si-O-H species relative to the process in water as can be seen in Fig. 5(c). However, it is also evident from Fig. 5(c) and (d) that surfaces exposed to H_2O_2 have a lower Si—H content, which is in agreement with previous observation showing that H_2O_2 molecules only lead to the formation of Si—O—H species [75]. It should be noted that the use of aqueous H_2O_2 without diamond abrasives was just to demonstrate the chemical effect of the slurry, where no Si or C atoms were removed from SiC. Similar MD simulation studies were performed on other materials such as silicon, diamond, and quartz [48,49,52,53].

Similar characteristics were found when aqueous H_2O_2 was placed on the $(000\bar{1})$ C-face of 6H-SiC where the consumption of H_2O_2 was accompanied by the generation of C—O—H and C—H species. Similar observations have previously been made for ReaxFF simulations of diamond in aqueous H_2O_2 [52]. Fig. 6(a) presents the number of remaining water and H_2O_2 molecules (noting that different numbers of molecules were added in the simulation, see Table 2), while Fig. 6(b) presents the species generated on Si- and C-faces after 100 ps. Similar for both faces is the decrease in Si/C-H species with increasing H_2O_2 concentration. It is noted that more water molecules were retained on the C-face compared to the Si-face, as shown in Fig. 6(a), and this is accompanied by a higher amount of Si—H and Si—O—H species than C—H and C—OH species Fig. 6(b). This indicates that the reactivity of the C-atoms on the $(000\bar{1})$ C-face is lower than that of the Si-atoms (0001) on the Si-

Table 4
Parameters used in the lapping and polishing experiments.

Parameters	Values	
	Lapping	Polishing
Pad	Metal-resin composite plate (MD-Largo)	Fabrics plate (MD-Nap)
Normal load (N)	15	10
Disc rotational speed (rpm)	240	180
Holder rotational speed (rpm)	150	150
Duration (min)	24	180
Flow rate of slurry (ml/min)	4	1
Abrasive size (nm)	250, 500, 1000 & 3000	
Abrasive concentration (wt%)	1.0	
GO concentration (wt%)	0.25	

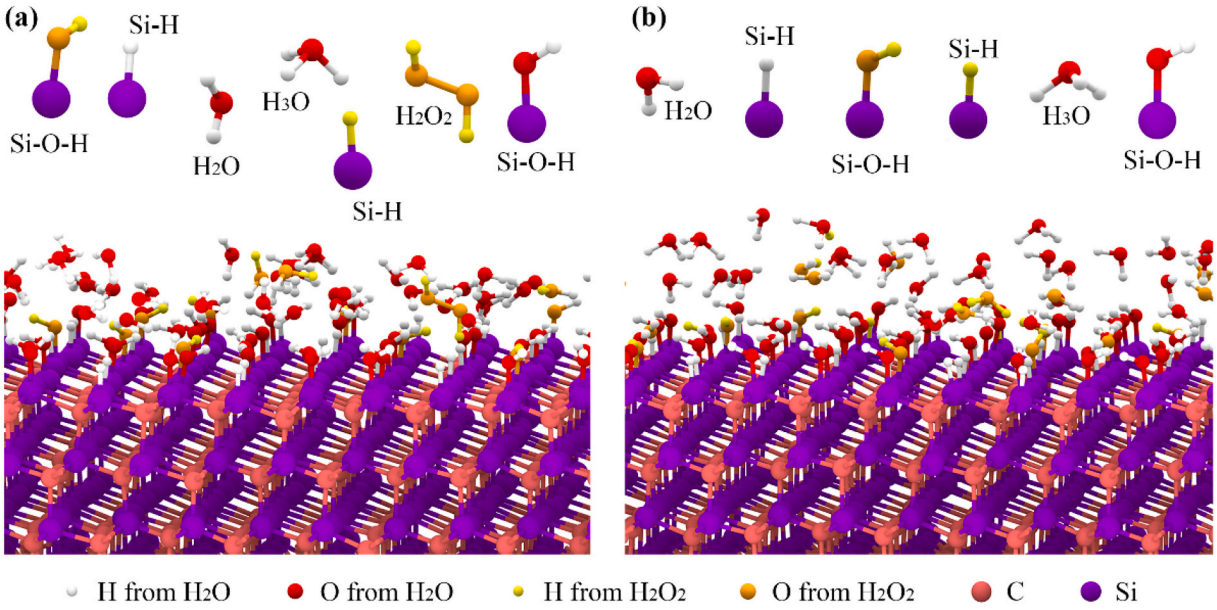

Fig. 4. Chemical species formed in the presence of aqueous H_2O_2 solution (16 wt%) on the (0001) Si face of 6H-SiC after (a) 40 ps, and (b) 100 ps. H_2O_2 molecules are observed in (a), indicating that the chemical reaction is still ongoing. However, in (b), H_2O_2 molecules are no longer observed, suggesting that the reaction between the SiC surface and H_2O_2 is complete after 100 ps.

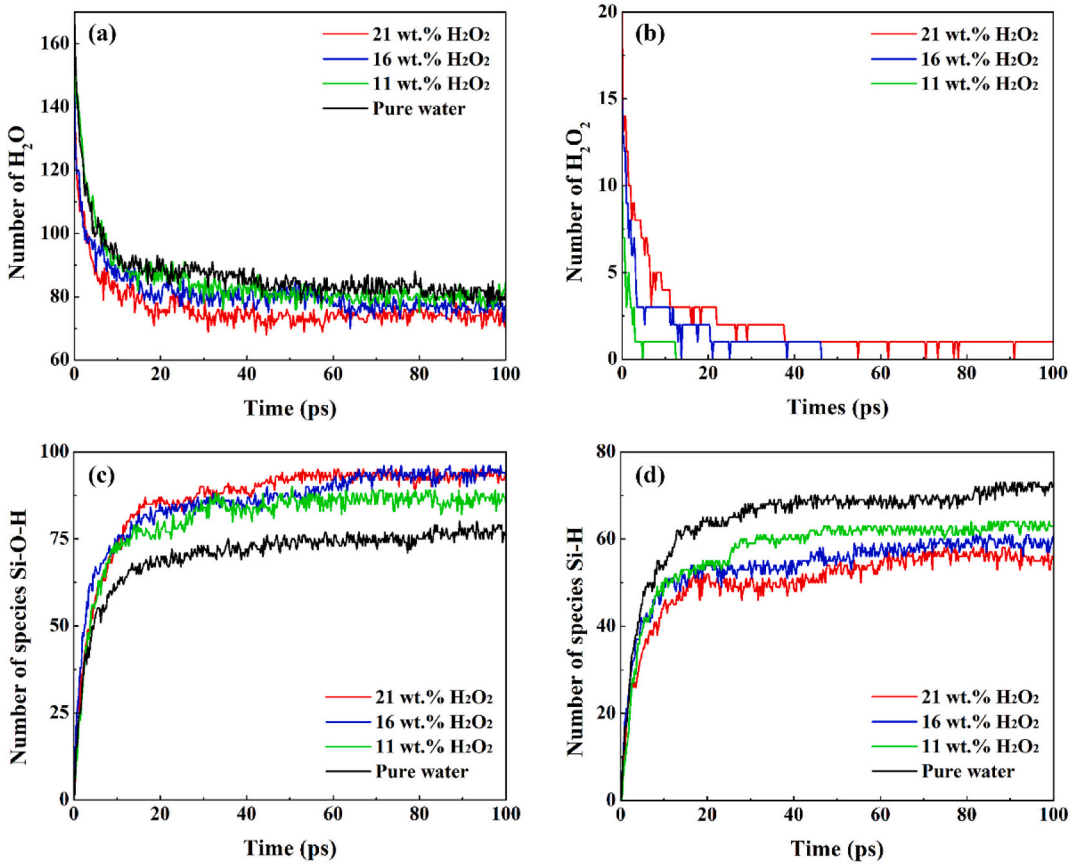

Fig. 5. Number of (a) H_2O, (b) H_2O_2, (c) Si—O—H and (d) Si—H species on Si-face of SiC plotted against reaction time when different H_2O_2 concentrations were used.

face in aqueous H_2O_2.

3.2. Material removal in CEP

A diamond abrasive was introduced into the simulation after 100 ps of equilibrium to simulate the materials removal in CEP using aqueous

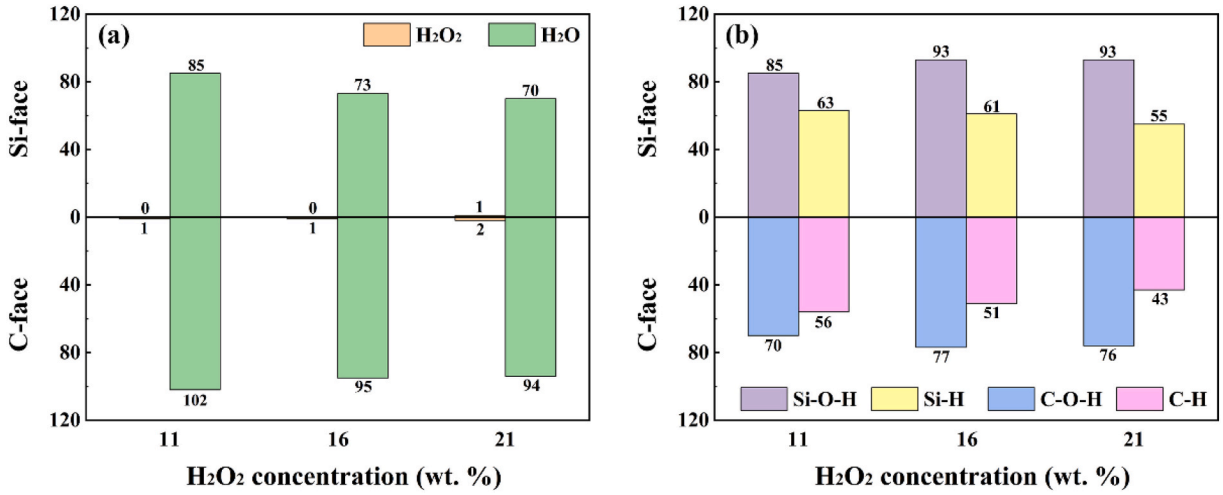

Fig. 6. Numbers of (a) H_2O_2 & H_2O molecules remaining, and (b) Si/C—O—H & Si/C—H species formed after the chemical reaction at 100 ps on Si- and C-faces of 6H-SiC, plotted against H_2O_2 concentration.

H_2O_2. The simulation was performed on both Si- and C-faces of the 6H-SiC single crystal to investigate the difference in their respective material removal process.

3.2.1. *Removal of a Si atom on Si-face*

Fig. 7 displays snapshots of the removal of a Si atom in a CEP process. All the atoms involved in the removal are labeled with subscripted numbers according to their order of appearance to track their movement, e.g., the Si atom was marked as Si_0. Before the removal process, Si_0 is present as a Si-O-H species on the surface. When the abrasive moves down, atomic rearrangements on the surface are observed, which eventually leads to the formation of a Si_0-O_2-C_4 interfacial species (the C_4 atom was from diamond) at 57.50 ps. Similar interfacial bridge species have previously been observed using a silica abrasive on a Si

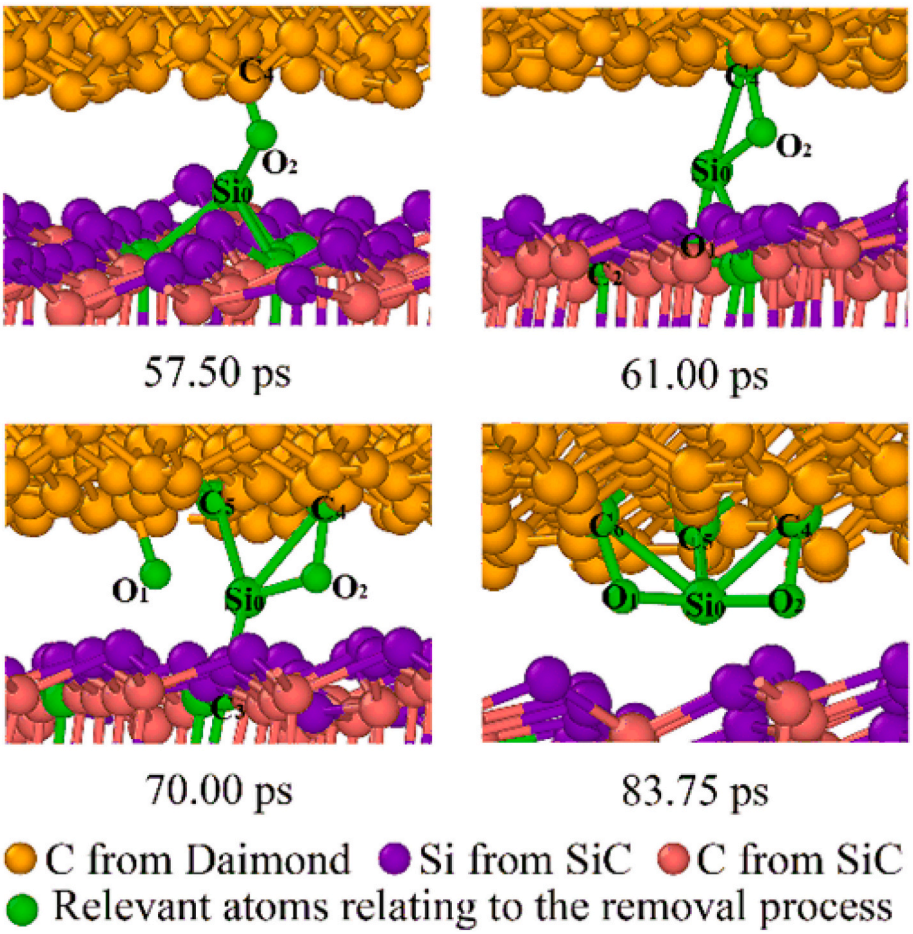

Fig. 7. Illustration of the removal of a Si atom from the Si-face of a 6H-SiC substrate. For clarity, only diamond abrasive, 6H-SiC substrate and relevant O and H atoms are shown, and the reacted atoms are numbered with subscripts. The O_1—C_6 and O_2—C_4 bonds may be an artefact of the cut-off length used in this study.

surface [49]. Following this, Si_0 is pulled closer to the abrasive causing the Si_0-C_2 bond to break at 61 ps. As the abrasive moves and causes mechanical abrasion, Si_0 is pulled further out to form a bond with C_5 of the abrasive, leading to the breakage of Si_0-C_1 at 65.50 ps. Subsequently a second Si_0-O_1-C_6 bridge species form as the Si_0-C_3 breaks. The detachment of Si_0 from 6H-SiC is completed at 83.75 ps. To summarize the process, Si atoms on the original surface is oxidized and the formation of Si—O—C bridge species leads to the breaking of Si—C bonds at its base. Some of the O atoms 'intrude' into the substrate to form Si—O—C bonds, resulting in the breaking of Si—C bonds [52]. Eventually, Si atoms are bonded to C atoms in the abrasive, either directly or via Si—O—C bonds and removed.

3.2.2. Removal of a C atom on Si-face

MD simulation was also performed to show the removal of a C atom on the Si-face. As shown in Fig. 8, all the involved atoms are labeled with subscripted numbers in sequence to trace their movement. Unlike Si atoms, C atoms are less exposed at the surface at the beginning and are connected to four Si atoms. During the removal of Si atoms, O atoms 'intrude' into the substrate to form Si—O—C bonds [52] as can be observed after 53.25 ps, where C_0 is connected to O_1-Si_1, as well as to Si_2, Si_3, and Si_4. At 54.50 ps, the C_0-Si_4 bond breaks. O_2 from a OH group of the slurry binds to C_0 and Si_2 forming a C_0-O_2-Si_2 species at 58.00 ps. Thereafter, C_0-O_1 breaks as Si_1 is removed by the abrasive. C_2 in the abrasive is then bonded to C_0, leading to the breakage of C_0-Si_2. At 86.75 ps, a C_2-C_0-O_2-Si_3 chain is formed and C_0 is removed from the substrate. In has previously been observed that C-atoms in diamond can be removed in the form of C-chains [52] and a study on the wear of SiC revealed C-removal through hydrocarbons [60]. In summary, the process involves the initial removal of some Si atoms, following by reaction of O atoms with C atoms in the SiC substrate and their connection to C atoms in the abrasive through C—C bonds, and finally their removal.

3.2.3. The removal of 6H-SiC

The processes described in Sections 3.2.1 and 3.2.2 form the basic material removal mechanism of Si and C atoms in 6H-SiC. Our simulation results indicate that the removal of Si and C atoms on the Si-face of 6H-SiC is similar to that on the C-face. Therefore, the removal process on the C-face of SiC is not illustrated and described in this paper. It should also be noted that all processes of removal are at the initial stage of the CEP. The surface is expected to undergo changes or become more complex as the number of atoms removed increases during polishing. Nevertheless, the fundamental mechanism of removal is expected to remain the same.

Fig. 9 shows the number of all species plotted against the processing time during CEP of the (0001) Si-face. It is seen that while the number of Si—O—H species decreases over polishing time, the number of other species increase or remain relatively unchanged. This indicates the continuous conversion of Si—O—H into O—Si—O or Si—O—Si. The Si atoms were eventually removed by the abrasive by means of forming Si—C_{abr} or Si—O—C_{abr} bonds (here C_{abr} represents the C atoms from diamond abrasive and C_{sub} represents the C atoms from 6H-SiC substrate). Regarding the removal of C atoms, as no C atoms are initially exposed to the Si-face, the C—O—H species start appearing after approximately 50 ps but remain low in number. After Si atoms are removed, which leads to the exposure of C atoms and the formation of

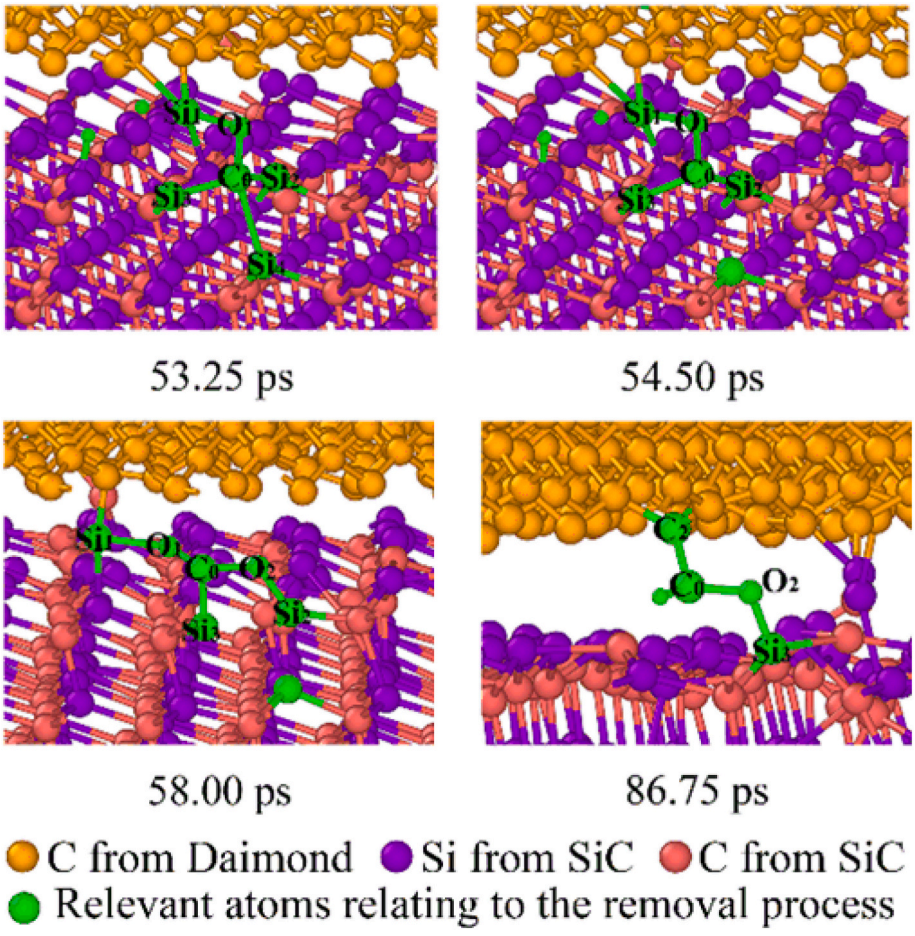

Fig. 8. Illustration of the removal of a C atom from the Si-face of a 6H-SiC substrate. For clarity, only diamond abrasive, 6H-SiC substrate and relevant O and H atoms are shown, and the reacted atoms are numbered with subscripts.

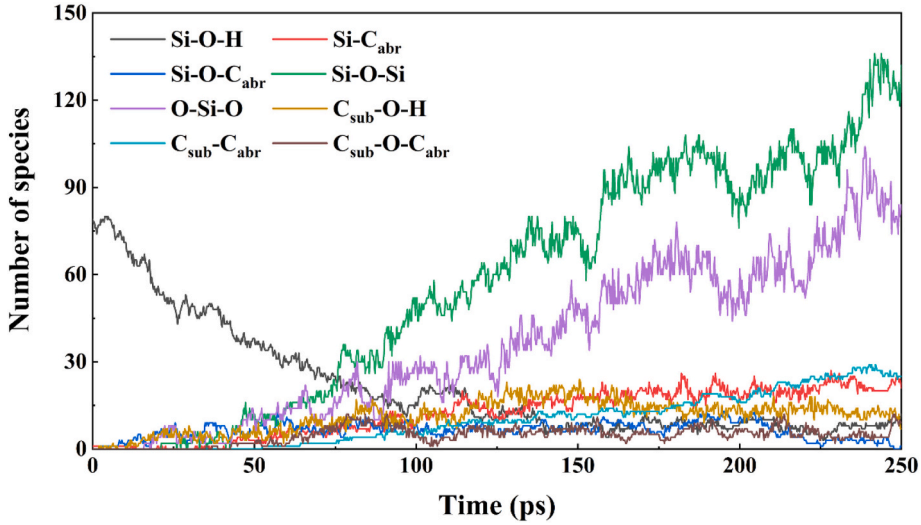

Fig. 9. Variation in the number of species on Si-face as a function of time during CMP with a suspension containing 16 wt% H_2O_2.

C_{sub}—O—H or C_{sub}—O—Si, the C atoms are then removed by the abrasion through forming mainly C_{sub}—C_{abr} and to a lesser extent C_{sub}—O—C_{abr} species. Please note that the presence of Si—O—Si and O—Si—O species might be attributed to the formation of an oxide layer dominated by Si—O bonds on the interface through continuous abrasion, which agrees with previous experimental studies [20–22,77].

3.3. The removal of Si- and C-face

Fig. 10 shows the atomic arrangement of 6H-SiC for both Si- and C-faces during CEP, obtained using the Identify Diamond Structure modifier. It should be noted that in this figure only the atoms of 6H-SiC are present and other atoms from CEP suspension and abrasive are removed for simplicity. The result shows that the initially ordered top surface atoms of 6H-SiC become increasingly disordered as the diamond abrasive moves over the surface, with the level of disorder increasing with polishing time. At the same time, with an increased H_2O_2 concentration, the degree of disorder becomes more pronounced. This is because the increase in concentration of H_2O_2 produced more Si-OH and C-OH species, and this in turn lead to the generation of more disordered atoms. However, it's difficult to see the difference in the numbers of disordered atoms visually between different H_2O_2 concentrations.

The number of disordered atoms on the two surfaces are thus quantified and presented in Fig. 11. Apparently, a higher H_2O_2 concentration results in more disordered atoms generated during polishing. There are fewer disordered atoms on the C-face than on the Si-face.

Fig. 12 displays the number of atoms with $d > 4.5$ Å which was calculated using Eq. (2). Here, we define these atoms as being removed during polishing. Similar to the results presented in Fig. 11, an increased H_2O_2 concentration leads to an increase in the number of atoms being removed. The number of the removed atoms of Si-face is greater than that of C-face.

4. Experimental results

To validate the findings from MD simulation, chemically enhanced polishing (CEP) and lapping (CEL) experiments were carried out. During CEP and CEL, the same chemical suspensions were used. The major difference between CEP and CEL is the pads used. In CEL a metal-resin composite disc (MD-Largo) was used, while in CEP a fabric plate (MD-Nap) was employed. Thus, CEL had a more intense mechanical abrasion than CEP due to the use of a more aggressive pad, while in CEP chemical effect plays a more dominant role. Detailed experimental conditions can be found in Table 4.

Fig. 13 shows the material removal rate (*MRR*) and surface roughness obtained from CEL and CEP of 6H-SiC, with the results in (a) and (b) obtained from polishing and (c) and (d) from lapping. From Fig. 13(a) and (c), it is seen that in both polishing and lapping, *MRR* increased with the increase in abrasive size. The *MRR* in CEL consistently exceeds that in CEP. Additionally, the *MRR* on C-face is higher compared to Si-face in CEL, while in CEP, opposite results were obtained, with the *MRR* on the Si-face being higher than that on the C-face. As shown in Fig. 3(b) and (d), polishing produced a better surface quality on C-face than Si-face, while lapping generated similar surface quality on both faces.

5. Discussion

The MD simulation clearly demonstrates that Si and C atoms can be removed from a 6H-SiC single crystal substrate through forming Si_{sub}—O—H and Si_{sub}—H as well as C_{sub}—O—H and C_{sub}—H species with an aqueous H_2O_2, followed by the formation of Si_{sub}—C_{abr} and Si_{sub}—O—C_{abr} as well as C_{sub}—C_{abr} and C_{sub}—O—C_{abr} during mechanical abrasion, as evident in Fig. 9 and displayed in Figs. 7 and 8. The chemical effect involved in the removal can be enhanced through increasing the concentration of H_2O_2. The results in Figs. 11 and 12 strongly support this finding. The influence of H_2O_2 concentration would reach a limit when the surface is saturated with Si—OH (and C—OH) groups. An increase in H_2O_2 concentration from 16 % to 21 % did not result in a significant increase in the number of disordered atoms on the Si-face.

As mentioned earlier, there exist contradictory experimental results on the removal of Si- and C-faces in the literature of the abrasive machining of SiC single crystals: one side indicated that Si-face was easier to be removed than C-face [29–31], and the other suggested otherwise [32–36]. Our simulation has shown that the use of H_2O_2 in suspension could cause atomic disorder in both Si- and C-faces, as shown in Fig. 10, but the chemical effect of H_2O_2 on the Si-face is stronger than that on the C-face for the same concentration used, as shown in Figs. 11 and 12, where the number of disordered atoms on Si-face are much higher compared to C-face. With an increased H_2O_2 concentration, the degree of disorder becomes more pronounced. The increase in concentration of H_2O_2 produced more Si-OH and C-OH species, and this in turn led to the generation of more disordered atoms.

The major difference between the two faces of SiC is the order of the Si and C atomic layers. The Si-face is characterized by Si atoms occupying the topmost layer, with each Si atom being bonded to three C atoms in the layer immediately below. On the C-face, the top layer consists of C atoms, each of which is bonded with three Si atoms in the

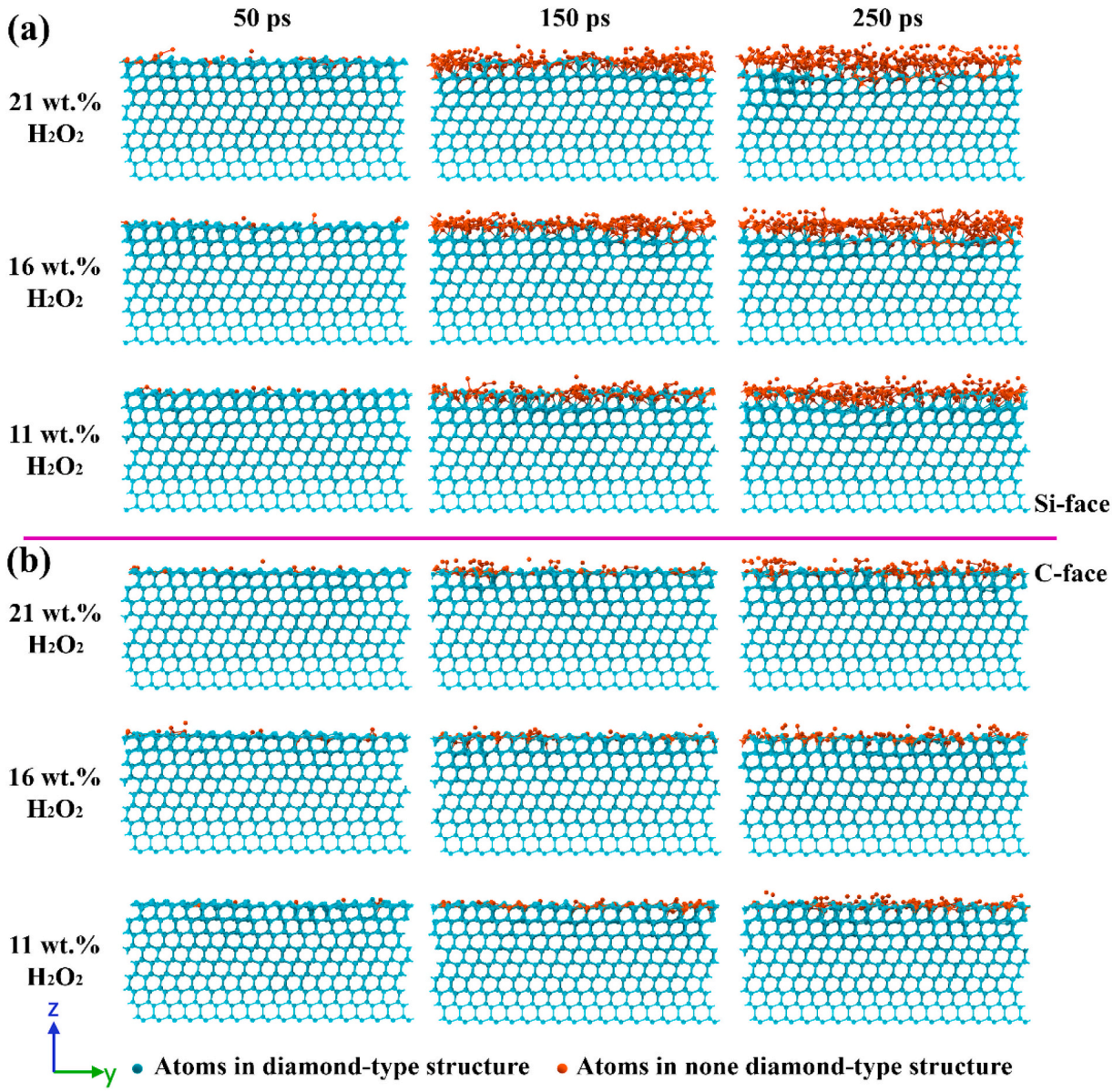

Fig. 10. Snapshots of the 6H-SiC substrate during sliding with different H_2O_2 concentrations on (a) Si- and (b) C-faces at different times, where pressure is 40 GPa and sliding velocity is 50 m/s. Only atoms in 6H-SiC are shown for clarity.

next atomic layer. Our MD simulation of the chemically enhanced polishing has indicated that a higher number of Si—O—H species are generated compared to C—O—H species during the chemical treatment. Furthermore, during the removal process, Si atoms are removed from the SiC substrate through multiple Si—O—C_{abr} and Si—C_{abr} bridging species while C atoms are removed via a single C_{abr}—C bridging species. In both processes, a single bridge species connects the atom being removed to the SiC substrate (e.g., a Si—C bond in the case of Si removal and a C—O—Si bond in the case of C removal). The lower bond energy of the Si—C bond compared to a C—O or Si—O bond [78] additionally benefit removal of Si atoms compared to C-atoms. Overall, both the higher concentration of Si—OH species at the surface that can initiate the removal process, and stronger Si—O bonds generated between the abrasive and Si on the Si-face, produce a higher driving force to overcome the Si—C bonds.

Fig. 13 show the Material removal rate (*MRR*) and surface roughness (*Sa*) after polishing and lapping, respectively. During chemical enhanced polishing, the *MRR* of the Si-face was found to be higher than that of the C-face, as demonstrated in Fig. 13(a), which is in good agreement with the simulated results. The notable difference in *MRR* can be ascribed to the use of soft fabric in the polishing process, which resulted in a reduction of mechanical effect for material removal, thereby enhancing the chemical effect. The stronger synergistic interaction between the chemical and mechanical actions on the Si-face enhances the material removal rate compared to the C-face. In the case of lapping, where a much more aggressive polishing pad was utilized, the mechanical effect predominated over the chemical effect. Consequently, the removal rate on the C-face was higher than that on the Si-face, as demonstrated in Fig. 13(c). On the other hand, in the case of lapping in this work, where a much more aggressive polishing plate was used, the chemical effect in the process was overwhelmed by the mechanical effect, therefore the removal rate on C-face was higher than that on Si-face, as demonstrated in Fig. 13(c). Although our nanoindentation tests showed that the hardness values of Si- and C-face are remarkably similar, the coefficient of friction of Si-face is much lower than that of C-face, as shown in Fig. 14. This suggests that a greater lateral or shear force is induced in the removal of the C-face than the Si-face, leading to easier mechanical removal. In addition, the surface finish of the C-face

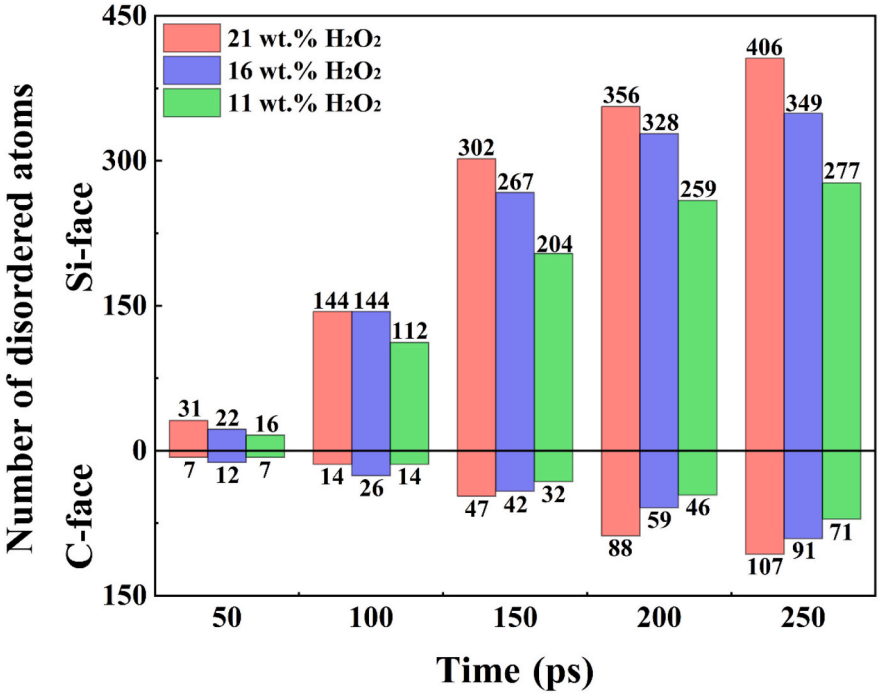

Fig. 11. Variation of the numbers of disordered atoms during CMP with different H_2O_2 concentrations.

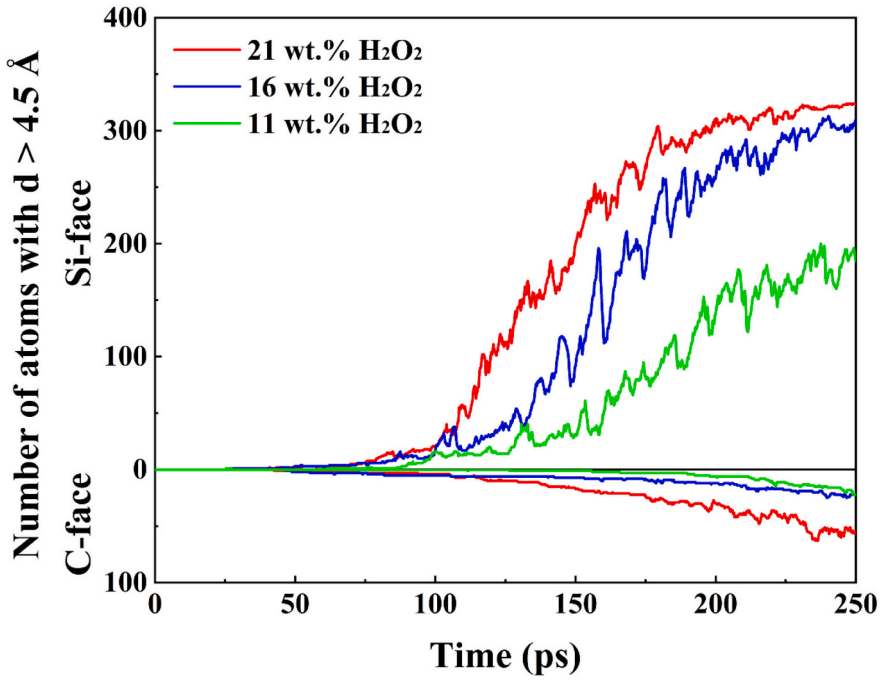

Fig. 12. Change in the number of atoms with d > 4.5 Å during sliding on Si- (up) and C-faces (down) with different H_2O_2 concentrations over time.

generated by polishing is superior to that of the Si-face, as shown in Fig. 13(b). This is because a higher *MRR* during polishing usually results in a poorer surface finish.

The findings of this study offer valuable insights for designing effective material removal processes for 6H-SiC single crystals. In processes where the chemical effect and mechanical effect are in competition, such as CMP, it is suggested to prioritize polishing the Si-face to achieve a higher removal rate. However, if a superior surface finish is the objective, polishing the C-face is recommended. In cases where the mechanical removal dominates over the chemical effect, as in the case of CEL, lapping on the C-face is advised for achieving a higher removal rate.

6. Conclusions

In this study, ReaxFF MD simulation was carried out to gain insight into the chemical effect in the polishing of 6H-SiC with H_2O_2 solution. The main findings of this study are summarized below:

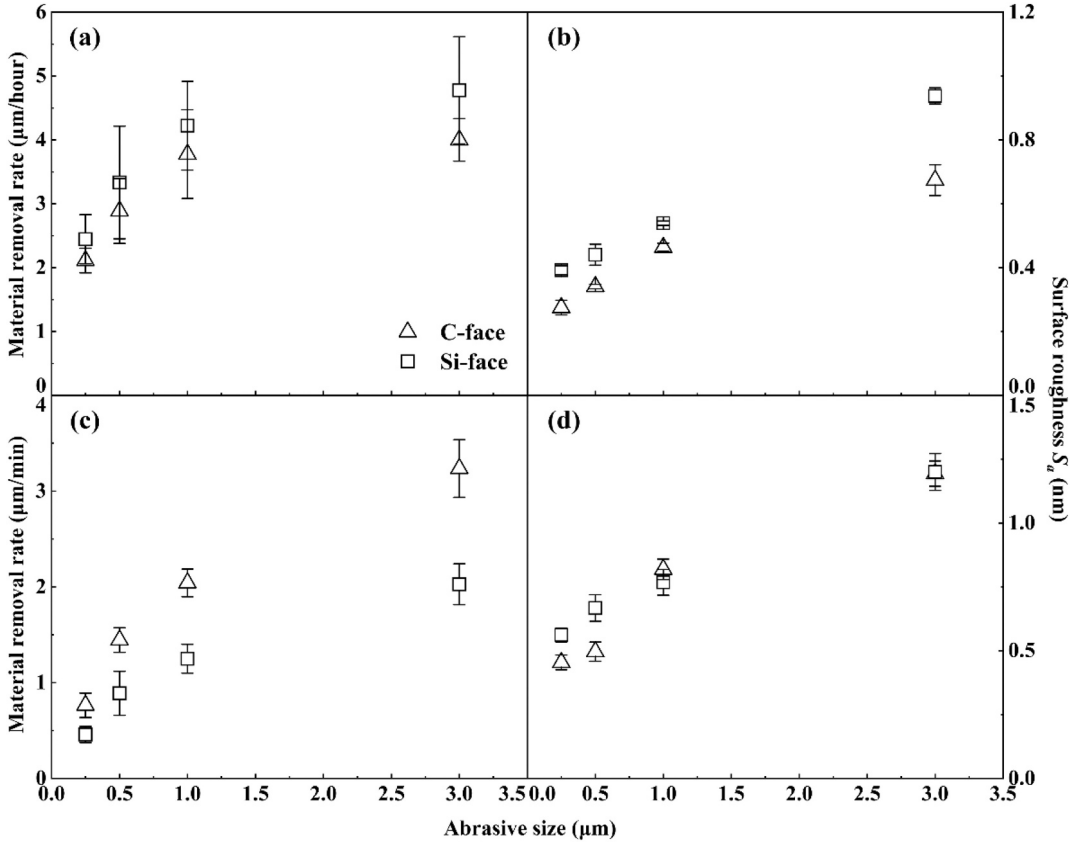

Fig. 13. (a) Material removal rate (MRR) and (b) surface roughness (Sa) after polishing, (c) MRR and (d) surface roughness (Sa) after lapping, plotted against abrasive size.

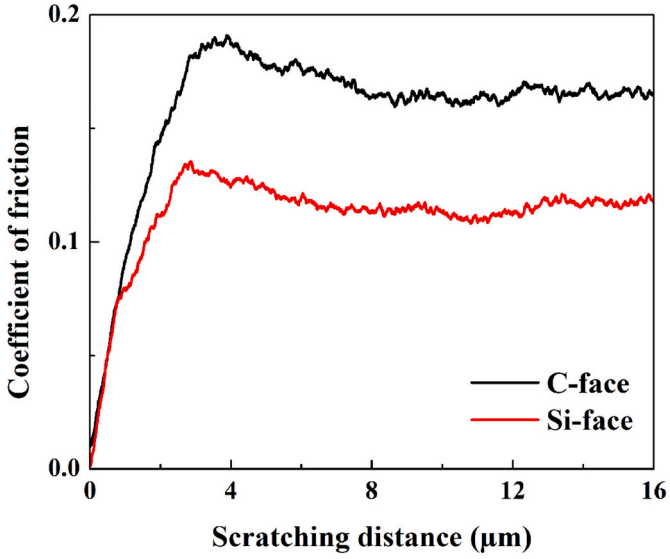

Fig. 14. Coefficients of friction obtained from nanoscratching on C- and Si-faces.

- The formation of Si—O—H and Si—O—Si species in the substrate facilitates the removal of Si atoms during the polishing process. Similarly, the formation of C—O—H and C—O—Si species in the substrate aids in the removal of C atoms.
- The utilization of H_2O_2 as a polishing suspension results in the generation of Si-O-H and C-O-H species. The impact of its chemical effect on material removal is influenced by the concentration of H_2O_2. A higher concentration of H_2O_2 yields a stronger chemical effect, up to a certain threshold concentration.
- The material removal process in the polishing involves a combination of chemical reaction and mechanical abrasion. The chemical effect of H_2O_2 is observed on both the Si-face and C-face, but it demonstrates a more pronounced influence on the Si-face compared to the C-face.
- The experimental results indicate that when the chemical effect is comparable to the mechanical removal, the removal rate of the Si-face is higher than that of the C-face. However, when the mechanical removal becomes more dominant, the C-face is more efficiently removed compared to the Si-face. These findings are in line with the MD simulation results concerning the chemical effect of H_2O_2 on both faces.

Declaration of competing interest

The authors declare that they have no known competing financial interests or personal relationships that could have appeared to influence the work reported in this paper.

Acknowledgement

The authors would like to thank Prof. Debra Bernhardt, Drs. Jeff Yun Huang, Xiaoming Sun, Yu Yin and Grant Edwards at The University of Queensland (UQ) for technical supports and valuable discussions. They would also like to acknowledge the support from the NCI National Facility resources at QCIF UQ for computation and the Queensland node of the Australian National Fabrication Facility (ANFF) for AFM characterization. This work is sponsored by the Australian Research Council under the Discovery Projects Program (DP210102061).

Appendix A. Supplementary data

Supplementary data to this article can be found online at https://doi.org/10.1016/j.jmapro.2023.10.056.

References

[1] Ivanov P, Chelnokov V. Recent developments in SiC single-crystal electronics. Semiconductor Sci Technol 1992;7:863.
[2] Nakamura D, Gunjishima I, Yamaguchi S, Ito T, Okamoto A, Kondo H, et al. Ultrahigh-quality silicon carbide single crystals. Nature 2004;430:1009–12.
[3] Yoon D-H, Reimanis IE. A review on the joining of SiC for high-temperature applications. J Kor Ceram Soc 2020;57:246–70.
[4] Ma G, Li S, Liu F, Zhang C, Jia Z, Yin X. A review on precision polishing technology of single-crystal SiC. Crystals 2022;12:101.
[5] Wang P, Ge P, Gao Y, Bi W. Prediction of sawing force for single-crystal silicon carbide with fixed abrasive diamond wire saw. Mater Sci Semicond Process 2017;63:25–32.
[6] Wu ZH, Liu WD, Zhang LC, Lim S. Amorphization and dislocation evolution mechanisms of single crystalline 6H-SiC. Acta Mater 2020;182:60–7.
[7] Wu ZH, Zhang LC, Yang SY. Effect of abrasive grain position patterns on the deformation of 6H-silicon carbide subjected to nano-grinding. Int J Mech Sci 2021;211:106779.
[8] Alves LF, Gomes RC, Lefranc P, Pegado RDA, Jeannin P-O, Luciano BA, et al. SIC power devices in power electronics: an overview. In: 2017 Brazilian power electronics conference (COBEP). IEEE; 2017. p. 1–8.
[9] Zhang H, Tolbert LM, Ozpineci B. Impact of SiC devices on hybrid electric and plug-in hybrid electric vehicles. IEEE Trans Ind Appl 2010;47:912–21.
[10] Hinata Y, Horio M, Ikeda Y, Yamada R, Takahashi Y. Full SiC power module with advanced structure and its solar inverter application. In: 2013 twenty-eighth annual IEEE applied power electronics conference and exposition (APEC). IEEE; 2013. p. 604–7.
[11] Brenna M, Foiadelli F, Zaninelli D, Barlini D. Application prospective of Silicon Carbide (SiC) in railway vehicles. In: 2014 AEIT annual conference-from research to industry: the need for a more effective technology transfer (AEIT). IEEE; 2014. p. 1–6.
[12] Ni Z, Li Y, Liu C, Wei M, Cao D. A 100-kW SiC switched tank converter for transportation electrification. IEEE Trans Power Electron 2019;35:5770–84.
[13] Yakimova R, Petoral R, Yazdi G, Vahlberg C, Spetz AL, Uvdal K. Surface functionalization and biomedical applications based on SiC. J Phys D Appl Phys 2007;40:6435.
[14] Yang X, Yang X, Kawai K, Arima K, Yamamura K. Novel SiC wafer manufacturing process employing three-step slurryless electrochemical mechanical polishing. J Manuf Process 2021;70:350–60.
[15] Chen X, Liang Y, Cui Z, Meng F, Zhang C, Chen L, et al. Study on material removal mechanism in ultrasonic chemical assisted polishing of silicon carbide. J Manuf Process 2022;84:1463–77.
[16] Goel S, Luo X, Comley P, Reuben RL, Cox A. Brittle–ductile transition during diamond turning of single crystal silicon carbide. Int J Mach Tool Manuf 2013;65:15–21.
[17] Huang S, Li X, Zhao Y, Sun Q, Huang H. A novel lapping process for single-crystal sapphire using hybrid nanoparticle suspensions. Int J Mech Sci 2021;191:106099.
[18] Zhao D, Lu X. Chemical mechanical polishing: theory and experiment. Friction 2013;1:306–26.
[19] Luo H, Ajmal KM, Liu W, Yamamura K, Deng H. Polishing and planarization of single crystal diamonds: state-of-the-art and perspectives. Int J Extreme Manuf 2021;3:022003.
[20] Huang S, Li X, Mu D, Cui C, Huang H, Huang H. Polishing performance and mechanism of a water-based nanosuspension using diamond particles and GO nanosheets as additives. Tribol Int 2021;164:107241.
[21] Wang W, Zhang B, Shi Y, Zhou J, Wang R, Zeng N. Improved chemical mechanical polishing performance in 4H-SiC substrate by combining novel mixed abrasive slurry and photocatalytic effect. Appl Surf Sci 2022;575:151676.
[22] Lu J, Chen R, Liang H, Yan Q. The influence of concentration of hydroxyl radical on the chemical mechanical polishing of SiC wafer based on the Fenton reaction. Precis Eng 2018;52:221–6.
[23] Wang W, Xu Q, Liu W, Song Z. Effect of particle size distribution, pH, and Na+ concentration on the chemical mechanical polishing of sapphire and 4H-SiC (0001). ECS J Solid State Sci Technol 2022;11:044004.
[24] Zhang Q, Pan J, Zhang X, Lu J, Yan Q. Tribological behavior of 6H–SiC wafers in different chemical mechanical polishing slurries. Wear 2021;472:203649.
[25] Neslen C, Mitchel W, Hengehold R. Effects of process parameter variations on the removal rate in chemical mechanical polishing of 4H-SiC. J Electron Mater 2001;30:1271–5.
[26] Lee H, Jeong H. Chemical and mechanical balance in polishing of electronic materials for defect-free surfaces. CIRP Ann 2009;58:485–90.
[27] Heydemann V, Everson W, Gamble RD, Snyder D, Skowronski M. Chemi-mechanical polishing of on-axis semi-insulating SiC substrates. In: Materials science forum. Trans Tech Publ; 2004. p. 805–8.
[28] Zhou Y, Pan G, Shi X, Xu L, Zou C, Gong H, et al. XPS, UV–vis spectroscopy and AFM studies on removal mechanisms of Si-face SiC wafer chemical mechanical polishing (CMP). Appl Surf Sci 2014;316:643–8.
[29] Chen X-F, Xu X-G, Hu X-B, Li J, Jiang S-Z, Ning L-N, et al. Anisotropy of chemical mechanical polishing in silicon carbide substrates. Mater Sci Eng B 2007;142:28–30.
[30] Yiqing Y, Zhongwei H, Wenshan W, Huan Z, Jing L, Xipeng X. The double-side lapping of SiC wafers with semifixed abrasives and resin–combined plates. Int J Adv Manuf Technol 2020;108:997–1006.
[31] Cicero G, Catellani A, Galli G. Atomic control of water interaction with biocompatible surfaces: the case of SiC (001). Phys Rev Lett 2004;93:016102.
[32] Takamoto S, Yamasaki T, Ohno T, Kaneta C, Hatano A, Izumi S. Elucidation of the atomic-scale mechanism of the anisotropic oxidation rate of 4H-SiC between the (0001) Si-face and (000 1^{-}) C-face by using a new Si-OC interatomic potential. J Appl Phys 2018;123:185303.
[33] Lu J, Luo Q, Xu X, Huang H, Jiang F. Removal mechanism of 4H-and 6H-SiC substrates (0001 and 000 1) in mechanical planarization machining. Proc Inst Mech Eng Part B J Eng Manuf 2019;233:69–76.
[34] Yin T, Zhao P, Doi T, Kurokawa S, Jiang J. Effect of using high-pressure gas atmosphere with UV Photocatalysis on the CMP characteristics of a 4H-SiC substrate. ECS J Solid State Sci Technol 2021;10:024010.
[35] Shen J, Chen H, Chen J, Lin L, Gu Y, Jiang Z, et al. Mechanistic difference between Si-face and C-face polishing of 4H–SiC substrates in aqueous and non-aqueous slurries. Ceram Int 2022;45:5.
[36] Chen G, Du C, Ni Z, Liu Y, Zhao Y. The effect of surface polarity on the CMP behavior of 6H-SiC substrates. Russian J Appl Chem 2020;93:832–7.
[37] Yang SY, Zhang LC, Xie HT, Liu WD. Interaction potential function for the deformation analysis of potassium dihydrogen phosphate using molecular dynamics simulation. Comput Mater Sci 2021;187:110122.
[38] Yang SY, Zhang LC, Wu ZH. Effect of anisotropy of potassium dihydrogen phosphate crystals on its deformation mechanisms subjected to nanoindentation. ACS Appl Mater Interfaces 2021;13:41351–60.
[39] Yang SY, Zhang LC, Wu ZH. Subsurface damage minimization of KDP crystals. Appl Surf Sci 2022;604:154592.
[40] Yang SY, Zhang LC, Wu ZH. Characterization and criteria of phase transformations and lattice slipping in potassium dihydrogen phosphate crystals. J Am Ceram Soc 2021;104:5955–65.
[41] Yang SY, Zhang LC, Wu ZH, Webster RF, Kong C, Chang SLY. TEM-MD characterization of KDP deformation mechanisms under nanoindentation. J Eur Ceram Soc 2023;43:3844–8.
[42] Yang SY, Zhang LC, Wu ZH. An investigation on the nano-abrasion wear mechanisms of KDP crystals. Wear 2021;476:203692.
[43] Dai H, Wu W, Li P. Atomistic simulation on the removal mechanism of monocrystal silicon carbide with textured surface nano-machining in water lubrication. J Manuf Process 2023;98:95–112.
[44] Dai H, Hu Y, Wu W, Yue H, Meng X, Li P, et al. Molecular dynamics simulation of ultra-precision machining 3C-SiC assisted by ion implantation. J Manuf Process 2021;69:398–411.
[45] Van Duin AC, Dasgupta S, Lorant F, Goddard WA. ReaxFF: a reactive force field for hydrocarbons. Chem A Eur J 2001;105:9396–409.
[46] Chenoweth K, Van Duin AC, Goddard WA. ReaxFF reactive force field for molecular dynamics simulations of hydrocarbon oxidation. Chem A Eur J 2008;112:1040–53.
[47] Senftle TP, Hong S, Islam MM, Kylasa SB, Zheng Y, Shin YK, et al. The ReaxFF reactive force-field: development, applications and future directions. npj Comput Mater 2016;2:1–14.
[48] Wen J, Ma T, Zhang W, Psofogiannakis G, van Duin AC, Chen L, et al. Atomic insight into tribochemical wear mechanism of silicon at the Si/SiO_2 interface in aqueous environment: molecular dynamics simulations using ReaxFF reactive force field. Appl Surf Sci 2016;390:216–23.
[49] Wen J, Ma T, Zhang W, van Duin AC, Lu X. Atomistic mechanisms of Si chemical mechanical polishing in aqueous H_2O_2: ReaxFF reactive molecular dynamics simulations. Comput Mater Sci 2017;131:230–8.
[50] Chen L, Wen J, Zhang P, Yu B, Chen C, Ma T, et al. Nanomanufacturing of silicon surface with a single atomic layer precision via mechanochemical reactions. Nat Commun 2018;9:1–7.
[51] Wang M, Duan F. Atomic-level material removal mechanisms of Si (110) chemical mechanical polishing: insights from ReaxFF reactive molecular dynamics simulations. Langmuir 2021;37:2161–9.
[52] Guo X, Yuan S, Wang X, Jin Z, Kang R. Atomistic mechanisms of chemical mechanical polishing of diamond (100) in aqueous H_2O_2/pure H_2O: molecular dynamics simulations using reactive force field (ReaxFF). Comput Mater Sci 2019;157:99–106.
[53] Guo X, Yuan S, Huang J, Chen C, Kang R, Jin Z, et al. Effects of pressure and slurry on removal mechanism during the chemical mechanical polishing of quartz glass using ReaxFF MD. Appl Surf Sci 2020;505:144610.
[54] Yuan S, Guo X, Huang J, Gou Y, Jin Z, Kang R, et al. Insight into the mechanism of low friction and wear during the chemical mechanical polishing process of diamond: a reactive molecular dynamics simulation. Tribol Int 2020;148:106308.
[55] He Y, Yuan Z, Tang M, Sun J, Liu C, Gao X. Mechanism of chemical and mechanical mutual promotion in photocatalysis-assisted chemical mechanical polishing for single-crystal SiC. Proc Inst Mech Eng Part C J Mech Eng Sci 2022;236:24 (09544062221117953).
[56] Kawaguchi K, Ito H, Kuwahara T, Higuchi Y, Ozawa N, Kubo M. Atomistic mechanisms of chemical mechanical polishing of a Cu surface in aqueous H_2O_2: tight-binding quantum chemical molecular dynamics simulations. ACS Appl Mater Interfaces 2016;8:11830–41.
[57] Wen J, Ma T, Zhang W, Van Duin AC, Van Duin DM, Hu Y, et al. Atomistic insights into Cu chemical mechanical polishing mechanism in aqueous hydrogen peroxide

and glycine: ReaxFF reactive molecular dynamics simulations. J Phys Chem C 2019;123:26467–74.
[58] Yue D-C, Ma T-B, Hu Y-Z, Yeon J, van Duin AC, Wang H, et al. Tribochemical mechanism of amorphous silica asperities in aqueous environment: a reactive molecular dynamics study. Langmuir 2015;31:1429–36.
[59] Wang Y, Xu J, Ootani Y, Bai S, Higuchi Y, Ozawa N, et al. Tight-binding quantum chemical molecular dynamics study on the friction and wear processes of diamond-like carbon coatings: effect of tensile stress. ACS Appl Mater Interfaces 2017;9:34396–404.
[60] Wang Y, Yukinori K, Koike R, Ootani Y, Adachi K, Kubo M. Selective wear behaviors of a water-lubricating SiC surface under rotating-contact conditions revealed by large-scale reactive molecular dynamics simulations. J Phys Chem C 2021;125:14957–64.
[61] Plimpton S. Fast parallel algorithms for short-range molecular dynamics. J Comput Phys 1995;117:1–19.
[62] Stukowski A. Visualization and analysis of atomistic simulation data with OVITO–the open visualization tool. Model Simul Mater Sci Eng 2009;18:015012.
[63] Hoover WG. Canonical dynamics: equilibrium phase-space distributions. Phys Rev A 1985;31:1695.
[64] Mortier WJ, Ghosh SK, Shankar S. Electronegativity-equalization method for the calculation of atomic charges in molecules. J Am Chem Soc 1986;108:4315–20.
[65] Tersoff J. Modeling solid-state chemistry: interatomic potentials for multicomponent systems. Phys Rev B 1989;39:5566.
[66] Vashishta P, Kalia RK, Nakano A, Rino JP. Interaction potential for silicon carbide: a molecular dynamics study of elastic constants and vibrational density of states for crystalline and amorphous silicon carbide. J Appl Phys 2007;101:103515.
[67] Park C, Cheong B-H, Lee K-H, Chang K-J. Structural and electronic properties of cubic, 2H, 4H, and 6H SiC. Phys Rev B 1994;49:4485.
[68] Chang K-J, Cohen ML. Ab initio pseudopotential study of structural and high-pressure properties of SiC. Phys Rev B 1987;35:8196.
[69] Gibbs JW. Elementary principles in statistical mechanics: developed with especial reference to the rational foundations of thermodynamics. C. Scribner's sons; 1902.
[70] Capitani GC, Di Pierro S, Tempesta G. The 6H-SiC structure model: further refinement from SCXRD data from a terrestrial moissanite. Am Mineral 2007;92:403–7.
[71] Maras E, Trushin O, Stukowski A, Ala-Nissila T, Jonsson H. Global transition path search for dislocation formation in Ge on Si (001). Comput Phys Commun 2016;205:13–21.
[72] Cicero G, Galli G, Catellani A. Interaction of water molecules with SiC (001) surfaces. J Phys Chem B 2004;108:16518–24.
[73] Cicero G, Grossman JC, Catellani A, Galli G. Water at a hydrophilic solid surface probed by ab initio molecular dynamics: inhomogeneous thin layers of dense fluid. J Am Chem Soc 2005;127:6830–5.
[74] Cicero G, Catellani A. Towards SiC surface functionalization: an ab initio study. J Chem Phys 2005;122:214716.
[75] Morishita T, Kayanuma M, Nakamura T, Kato T. Cooperative reaction of hydrogen-networked water molecules at the SiC–H_2O_2 solution interface: microscopic insights from ab initio molecular dynamics. J Phys Chem C 2022;126:30.
[76] Li H, Shang H, Shi Y, Yakimova R, Syväjärvi M, Zhang L, et al. Atomically manipulated proton transfer energizes water oxidation on silicon carbide photoanodes. J Mater Chem A 2018;6:24358–66.
[77] Liu H-K, Chen C-CA, Hsieh P-C. Chemically grafted polyurethane/graphene ternary slurry for advanced chemical–mechanical polishing of single-crystalline SiC wafers. Int J Adv Manuf Technol 2022;120:7157–69.
[78] Greenwood NN, Earnshaw A. Chemistry of the elements. Elsevier; 2012.